protecting sheet flow of filtered air. The resulting particle speed in the aerosol beam centre was approximately 0.5 m/s. A second optical particle counter (Climet 500) was connected in parallel with the sample cell, in addition to the above mentioned. Particles ranging from 0.3 μm to 25 μm were counted and their size measured by both counters.

Representative data from 5 hours of continuous monitoring of the particle size distribution during BG aerosol generation are shown in Fig. 2. The steep slopes in the curves between 13.30 and 17.30 appear at times when the rotor was turned off and subsequently turned on again. Occasions when the smaller particle container was used to produce aerosols are seen after 17.30.

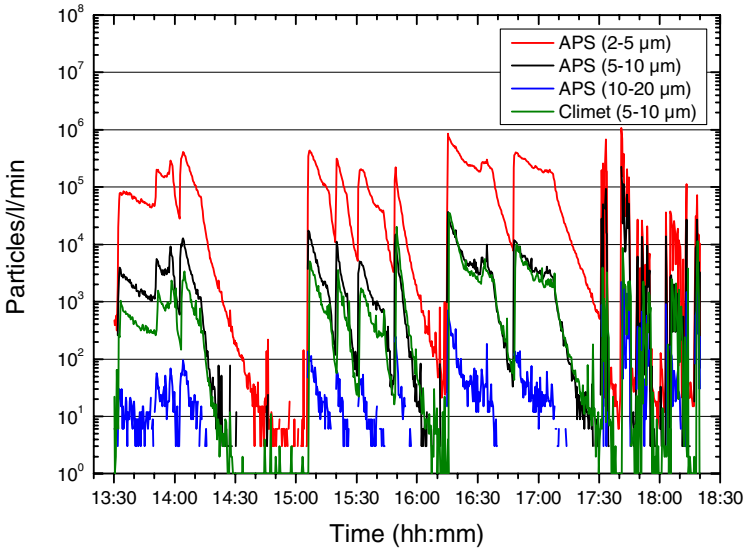

Figure 2. Representative data from the particle counters.

Optical setup

A top view of the optical setup is shown in Fig. 3. The air beam containing the biological particles was centred in the sample cell with two laser sources and the two optical collection probes mounted around the sample cell. The optical foci of the light sources and optical probes were arranged to overlap horizontally as well as vertically. A diode laser (LD) with a wavelength of 670 nm was used as optical trigger source. The LD could be modulated up to 100 kHz and the maximum output power was 3 mW. The focus of the beam was adjusted using an aspherical lens resulting in a beam diameter in the focus being smaller than 0.5 mm. The purpose of the LD was to generate scattered light when particles passed the focus. A fraction of this scattered light was collected by an optical probe with two lenses focusing the light into a fibre. The fibre output was directed onto a PMT detector used to trigger other sub-systems. When the signal from the PMT reached over a pre-set threshold it first turned off the trigger LD laser and simultaneously triggered a pulse from the ultraviolet (UV) laser as well as the PMT spectrometer array to collect data via the detection probe and the spectrograph.

The UV laser pulse, initiated by the presence of particles by the trigger laser, was focused onto the same spot as the trigger laser with a focusing probe consisting of two lenses. The

diameter of this focal volume was about 1 mm. The main part of the UV radiation was scattered by the particles in the focal volume, but some of the energy was absorbed by the aerosol particle to generate fluorescence. A fraction of the scattered radiation and the fluorescence were collected by the identical collection probes connected to fibres. A colour glass filter was placed in front of the spectrometer collection probe to block the scattered UV radiation while transmitting the fluorescence.

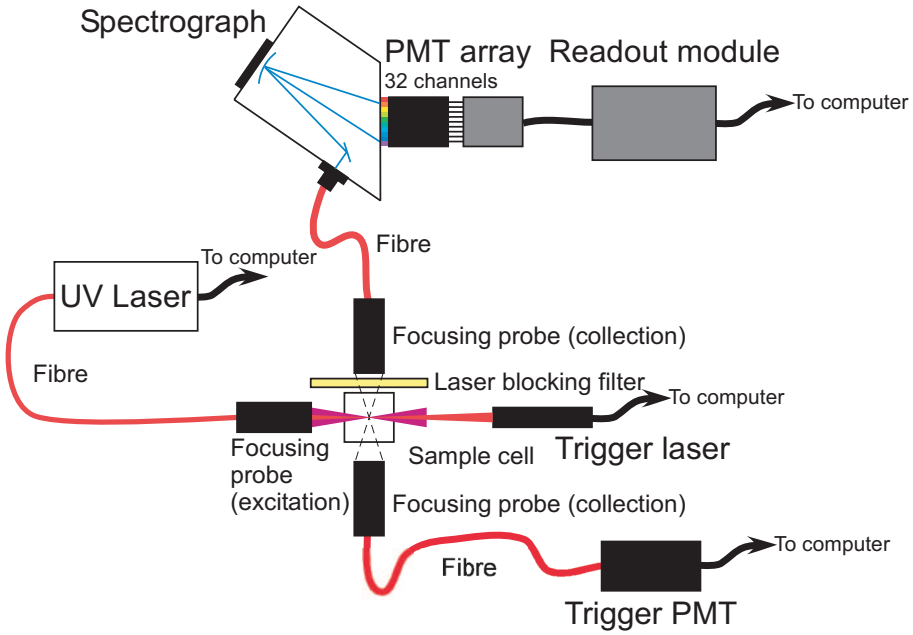

Figure 3. Schematic of the optical setup as seen from above (PMT = photomultiplier tube, UV = ultraviolet).

The spectrometer was constructed using a spectrograph and a 32 channel linear PMT array, and measured fluorescence spectra in the wavelength from 250 nm to 800 nm. The spectrograph consisted of a concave diffraction grating with a grating density of 405 lines/mm and a blaze wavelength of 350 nm. The spectrograph had a fibre-coupled input port well suited for the fibre from the collection probe and the length of the spectrum on the output port had a length comparable to the PMT array. For acquisition of the signal from the PMT array, a readout module was used. The readout module was externally triggered, as mentioned above, allowing for charge collection using integrating capacitors. The capacitance was $C = 33$ pF and the integration time was fixed to 1 μs. The voltage captured by the sample and hold circuit relate to the charge by $U = Q/C$ and represent the charge collected during 1 μs.

UV laser

A compact UV laser source was developed in order to reach wavelengths between 280 and 350 nm. It is based on parametric processes in nonlinear optical materials, which are pumped by a frequency-doubled passively Q-switched neodymium-doped yttrium aluminium garnet (Nd:YAG) laser emitting at 532 nm. The Nd:YAG laser medium was pumped by a broad-strip diode-laser at a wavelength of 808 nm and with a fast axis collimation package (dimensions

1 µm x 10 mm). The astigmatic beam profile of the diode laser was converted into an axially homogeneous irradiance profile with a beam twister [12]. The nearly symmetric beam was focused with a lens (focal length f = 10 mm) to a beam radius of 1 mm (e^{-2} intensity) inside the laser medium. The linear Nd:YAG laser cavity consisted of a 4 mm long Nd:YAG crystal (5 mm in diameter), a chromium-doped YAG (Cr:YAG) with an initial transmission of 34%, a Brewster window, and an output mirror with a reflectivity of 60%. The coatings of the laser rod were high reflective (HR) on one side and high transmissive (HT) on the other side at 1064 nm and HT on both sides at the 808 nm pump wavelength. The laser generated pulses with a full width at half maximum (FWHM) of 2.3 ns at a repetition rate of 100 Hz and an average power of 130 mW. The optical-to-optical efficiency from 808 to 1064 nm was nearly 10%. The beam-quality parameter M^2 and the beam radius was measured to 1.3 and 390 μm (e^{-2} intensity), respectively. In order to generate 532 nm radiation a 3 mm long periodically poled $KTiOPO_4$ (PPKTP) crystal designed for second harmonic generation (period, Λ = 9.01 μm), was placed in front of the output mirror and maintained at a temperature of 22°C. This crystal was anti-reflective (AR) coated for 1064 nm and 532 nm. A 50 % optical conversion efficiency was measured and a shortening of the pulse to 1.8 ns was observed, whilst the M^2 value was the same. The pulse shortening was a consequence of the second-order nonlinear process. The laser cavity and the doubling crystal were implemented on a copper block with a length of 35 mm, depicted in Fig. 4. The total length of the laser, including the diode bar, the beam twisting, the focusing optics, and the PPKTP crystal was 25 cm.

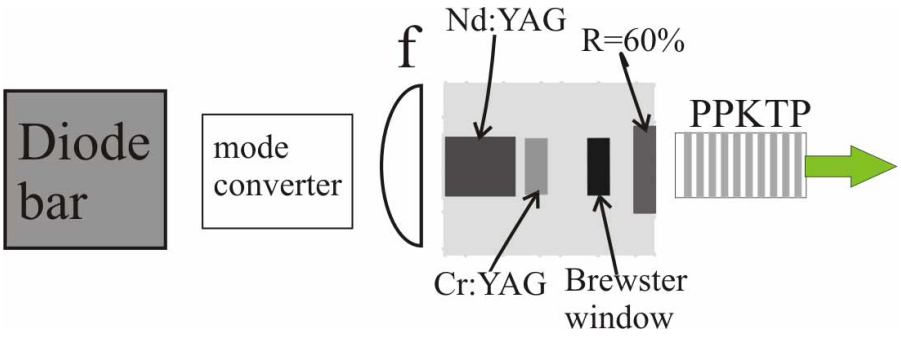

Figure 4. The diode-pumped Nd:YAG laser with frequency doubling (PPKTP = periodically poled potassium titanyl phosphate, Cr – Chromium, Nd = Neodymium, YAG = yttrium-aluminium garnet, R = reflectance).

The 532 nm beam was used to pump a singly resonant optical parametric oscillator (OPO) with intracavity sum-frequency mixing (SFM). A pump beam radius of 200 µm (e^{-2} intensity) was deployed with a telescope consisting of two lenses, f = 50 mm and f = -75 mm, separated 20 mm apart and at a distance of 50 mm from the second-harmonic generating PPKTP crystal. The parametric cavity consisted of an incoupling mirror, a second PPKTP crystal, a Type I β-barium borate (BBO) crystal, a dichroic mirror close to the cavity, and an output mirror (Fig. 5). By changing the grating period Λ of the PPKTP crystal it is possible to reach any wavelength between 280 and 350 nm for the cascaded parametric device. The grating period was Λ = 12.77 μm [13], giving a signal at 650 nm (idler at 2.9 μm). The SFM process in the BBO crystal between the signal and the pump generated UV radiation at 293 nm, whereas the idler was coupled out of the cavity.

The flat incoupling mirror M1 had a reflectivity of $R_S \approx 98\%$ at the signal wavelength, while transmitting approximately 95% of the pump. The PPKTP sample was made as an 8 mm long and 1 mm thick crystal and AR coated at the pump, the signal and the idler wavelengths, respectively. The 5 mm long AR-coated BBO crystal was cut and polished at an angle of $\theta = 42.1°$ relative to the crystallographic c-axis, for optimum birefringent phase-matching of the pump and the signal. A dichroic mirror was used to couple out the generated UV radiation. This mirror had a reflectivity of about 95% at 293 nm, while it was transmitting the signal, the idler and the pump waves. It was placed after the BBO at 45° with respect to the propagation direction. Finally, the flat output mirror M2 was AR coated for the pump and the idler, while it reflected 80% of the signal to keep the intracavity intensities below damage threshold of the coatings. The entire length of the OPO/SFM cavity was 26 mm.

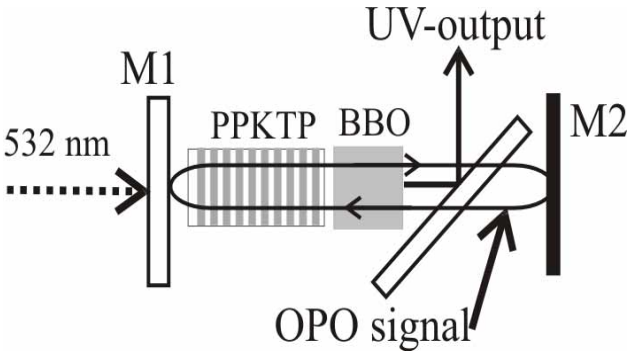

Figure 5. The setup of the OPO with intracavity SFM. (OPO – optical parametric oscillator, PPKTP = periodically poled potassium titanyl phosphate, BBO = beta barium borate, UV = ultraviolet, M = mirror)

Data collection system

The fluorescence acquisition system was triggered by the signal from the trigger PMT as described above. It was necessary to carefully adjust the timing of the events to assure that the PMT array data were collected in coincidence with the UV laser excitation. External timing circuits were used for this purpose. In practice, the internal delay of the lasers required that they were triggered in advance of the PMT array acquisition. However, the 1 μs long integration of PMT array signal started slightly before the UV laser pulse, in order to comprise the whole fluorescence signal which occurs in the ns range, partially within the excitation pulse. It is known that for similar species in solution the decay time of the fluorescence is typically in the order of 3 – 10 ns [6]. A schematic of the trigger PMT signal during a data acquisition cycle and the sequential triggering events is shown in Fig. 6. Each cycle to detect an aerosol particle and record and store its fluorescence spectrum included the following sequential events:

- at time t_1, the trigger PMT signal reaches the trigger level and the acquisition is initiated
- at time t_2, the trigger laser is turned off
- at time t_3, the PMT array detector acquisition is triggered
- at time t_4, the UV laser pulse is triggered
- at time t_5, the trigger laser (670 nm) is turned on again

The trigger laser was turned off during the acquisition to lower the background level. The gate time, i.e. the time the trigger laser is turned off (t_5- t_2), was adjusted to match with the maximum pulse repetition rate of the laser sources. The allowable rate of the data collection systems was above a kHz, i.e. well above the maximum 100 pulses/s of the lasers. The minimum cycle time as set by the aerosol injection system was longer than 1 ms, during which an aerosol at 0.5 m/s passes through the probe volume of about 1 mm. A way to prevent that light from each particle is collected more than once is simply to adjust the gate time. This was not of primary interest during these initial tests. Nevertheless, it was well taken care of by the comparably long gate time of more that 10 ms, as imposed by the laser constraints.

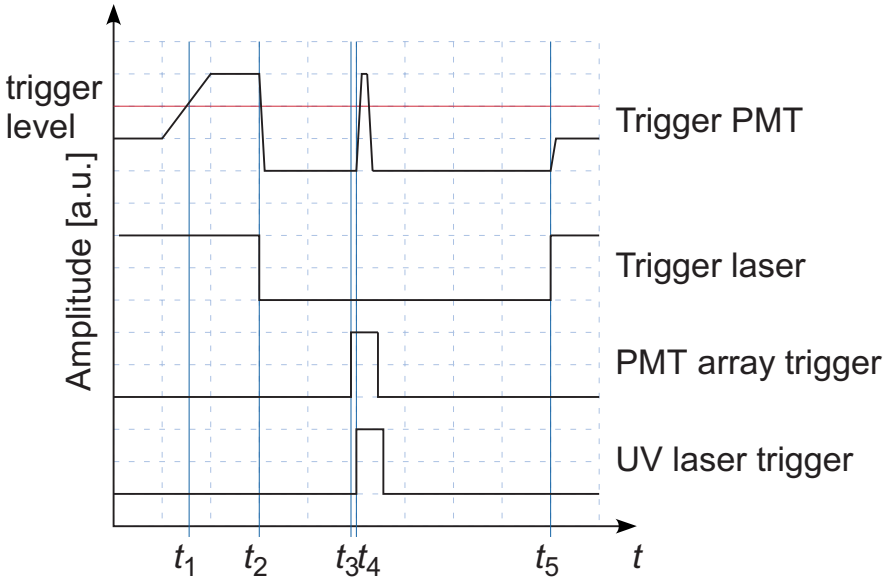

Figure 6. The schematics of the triggering sequence. (PMT = photomultiplier tube, UV = ultraviolet, t = time)

RESULTS AND DISCUSSION

The OPO was first characterized without the BBO crystal. The OPO threshold was reached with a pump pulse energy of 20 µJ and at 44 mW of launched power the signal pulse energy was 132 μJ, while the measured pump depletion was about 52%. At the maximum pump power the intracavity SFM produced a 293 nm beam with an output power of 3.2 mW, corresponding to a conversion efficiency of 7% in respect to the incident 532 nm pump, and a total conversion efficiency of 3.5% with respect to the IR (1064 nm). A single pass pumped OPO is inherently unidirectional; therefore the UV radiation was only generated in the direction of the pump wave vector. There was no measurable difference of the pulse length which was still 1.8 ns. The laser was coupled to the optical setup via an optical fibre. Some of the laser radiation was lost in the coupling in and out of the fibre. However, fibre coupling made it easy to switch between different lasers (other cases not discussed here) and the intensity levels were more than sufficient for these experiments. The trigger PMT signal from each complete cycle was recorded using a separate acquisition system collecting data at 500 kS/s. Diagrams from a typical BG recording are shown in Fig. 7. Here, the trigger laser was turned off at t_2- t_1 = 50 μs, the UV laser was triggered at t_4- t_1

= 100 μs and the gate time was t_5- t_2 = 20 ms. The threshold level in term of the detected voltage levels was 0.25 V as evident in the graphs from the first acquired values.

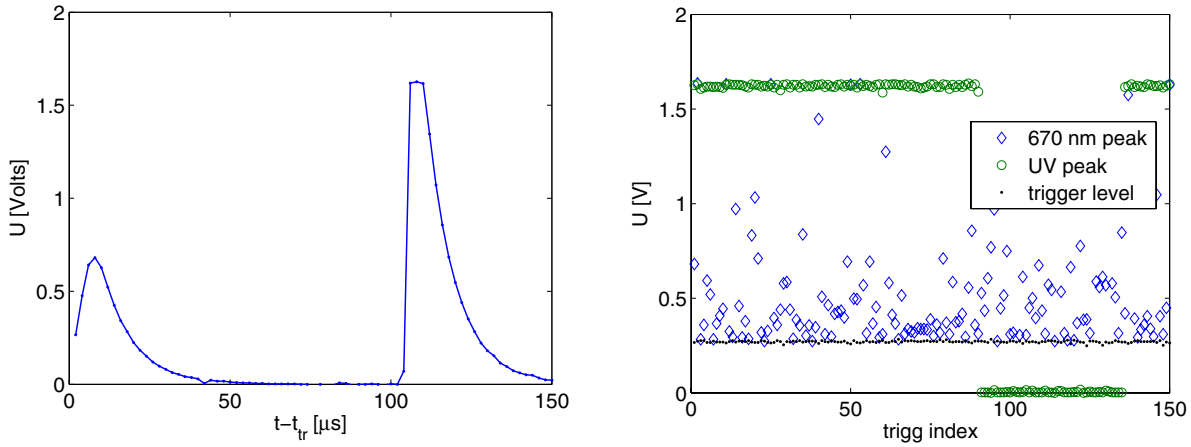

Figure 7. The diagram to the left shows a typical cycle as recorded with the trigger PMT detector and the diagram to the right shows extracted signals from a run incorporating trigger events associated with particles in the probe volume.

The first peak that appears in the PMT signal corresponds to the passage of the aerosol through the 670 nm laser focus and the second peak arises when the UV laser pulse is fired. Both the scattering signals originate from the same particle although the particle has passed the 670 nm laser focus before the UV laser fires. The explanation is that the focus is smaller for the trigger laser than for the UV laser. Additionally, the energy is much higher from the UV laser. The right-hand slope of the pulses is due to the electrical *RC* constant in the signal line connected to the preamplifier. A shunt resistor was tailored to yield a discharge time of approximately 10 μs. The left-hand slopes are steeper since a low series resistance allowed for a relatively fast charge up. The UV laser pulse has exceeded an upper dynamic limit of the system at about 1.6 V. This is why its peak value remains the same except for some triggers with the UV laser turned off during the run, as seen in the right hand graph. In addition to triggering the system, the trigger PMT signal can provide useful information about each event with regard primarily to size and particle velocity.

The laser and trigger system was used to record fluorescence spectra of various aerosol particles with spectral signatures similar to those of BWAs. Concomitant with the spectrum of individual particles, a background signal gradually evolved during the measurements (over several days). This background signal originated from contamination of the glass surfaces of the sample cell by aerosol particles. Therefore, before each measurement series with aerosols, a background signal was measured by collecting fluorescence spectra for a series of laser pulses exciting the bare sample cell, i.e. with the aerosol beam blocked/redirected. All spectra presented below are corrected by subtracting this obtained averaged background signal from the aerosol spectra.

Ovalbumin (OA) is a simulant used to represent viruses and protein based toxins since these usually lack the chemical entities (NADH, FAD, etc) of metabolism from biogenic particles. In water solution OA gives a relatively narrow fluorescence ranging from 300 to 425 nm with a peak at 345 nm and the dominating emission decay constant being 6.7 ns [6]. A representative series of spectra of the OA aerosol is displayed in Fig. 8 (left). The bar graph displayed to the

right in Fig. 8 is the resulting average spectrum obtained from the whole series. The overlaid line graph in the same figure shows the average fluorescence spectrum from OA in a water solution. One can detect a small shift of the emission maximum of approximately 0.5 – 1 channels (8 – 16 nm), otherwise the appearance of the signals is similar.

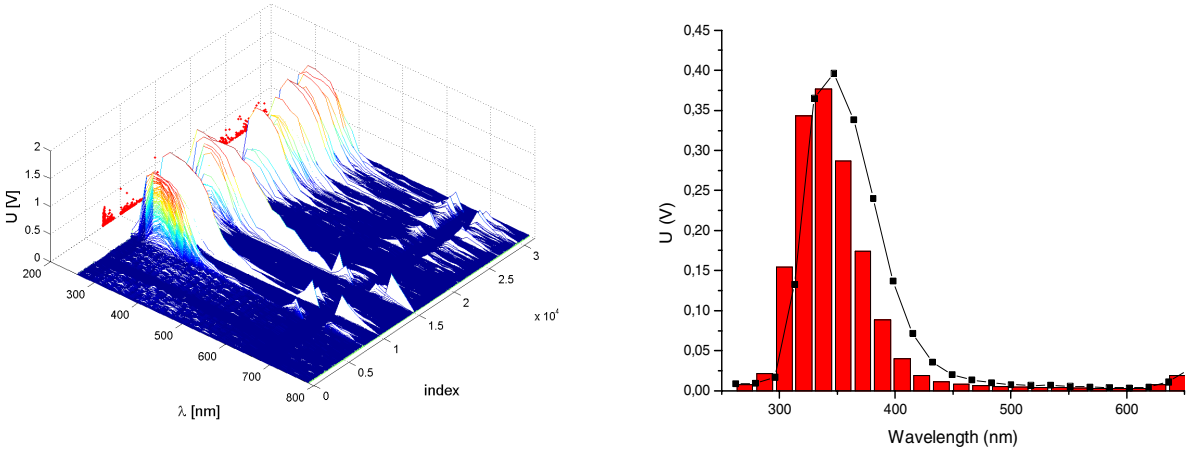

Figure 8. Fluorescence spectra of OA excited at 293 nm. The graph to the left shows consecutive spectra obtained during a measurement series. The "index" is the ordinal trigger after the start of the measurement i.e. it represents the different triggered events as the time progresses and particles are detected in the fluorescence volume. The graph to the right shows the averaged spectra of OA aerosols (bars) and OA in water solution (line), respectively.

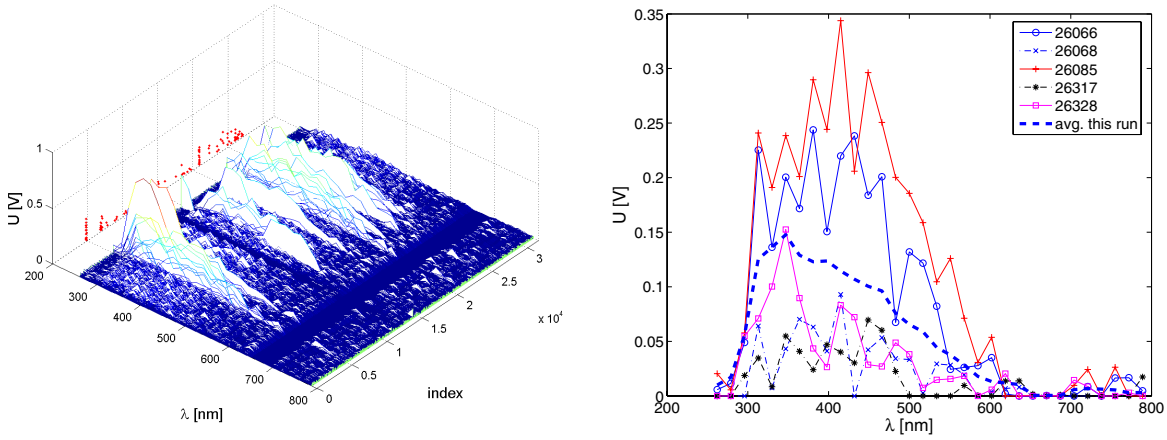

Figure 9. Fluorescence spectra of BT excited at 293 nm. The graph to the left shows consecutives spectra obtained during a measurement series. The "index" is the ordinal trigger after the start of the measurement i.e. it represents the different triggered events as the time progresses and particles are detected in the fluorescence volume. The graph to the right shows individual spectra for different trigger indices and the averaged spectra for the whole measurement series.

BG and BT was subjected to similar tests and showed similar event patterns. The analogous experiment with a series of events is shown in Figure 9 (left) for BT. The right graph shows the individual spectra of 5 typical events along with the average spectrum obtained from the whole series. Obviously the spectral information varies as the overall signal strength differs. Tentatively we assign the different signal strengths to particles of different sizes.

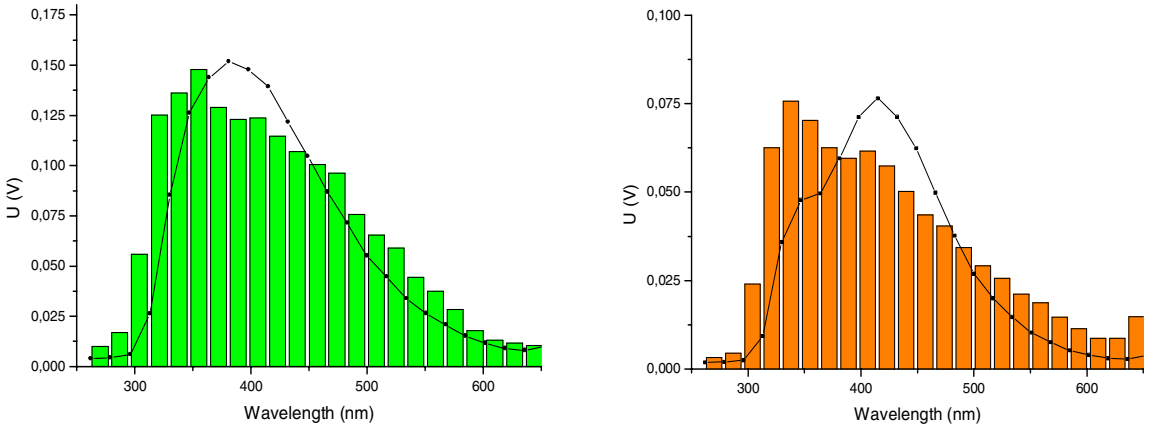

Figure 10. Average fluorescence spectra of BG (left) and BT (right) along with those obtained from solutions (excitation wavelength 293 nm).

Representative average spectra of BG and BT are shown in Figure 10 along with a typical spectrum obtained from the same sample in solution. As discussed in the introduction the physical and chemical state of the bio-particles in solution changes with time. Thus, we expect similar but not identical spectra, as observed in Fig. 10.

CONCLUSIONS

We have shown how an ultraviolet laser system designed to give laser radiation suitable for excitation of biological samples in conjunction with modern photonics detection technology enables the construction of a point-detection system for BWA detection. The fluorescence spectrum of individual bio-aerosol particles can be detected and it was further concluded that the spectrum is different from that obtained with the same kind of particles dissolved in water solutions. The used UV laser technology can be scaled up considerably to give more than 10 mJ/pulse in the relevant wavelength range [14]. With higher output power the desired laser technology can be used also for remote detection based on LIF [15-16]. The developed detection system provides resolved signatures, allows time-gating and is thereby readily adjusted for related LIDAR applications.

ACKNOWLEDGEMENTS

This work was supported by Swedish Defence Research Agencies (FMV and FOI).

REFERENCES

1. D. R. Walt and D. R. Franz, *Analytical Cemistry,* pp. 378 A-746 A (2000).
2. J. R. Lakowicz, *Principles of Fluorescence Spectroscopy*, 2nd ed. (Kluwer Academic/Plenum Publisher, New York, 1999).
3. S. C. Hill, R. G. Pinnick, S. Niles, Y.-L. Pan, S. Holler, R. K. Chang, J. Bottiger B. T. Chen, C.-S. Orr and G. Feather, *Field Analytical Chemistry & Technology* **3** (4-5), pp. 221-239 (1999).
4. M. Tiihonen, V. Pasiskevicius, F. Laurell, P. Jonsson, and M. Lindgren, *Proceedings of SPIE* **5332**, pp. 134-142 (2004).
5. M. Tiihonen, V. Pasiskevicius, F. Laurell, P. Hammarström, and M. Lindgren, *Proceedings of SPIE* **5240**, p.127-136 (2004).
6. P. Jonsson, F. Kullander, M. Nordstrand, T. Tjärnhage, P. Wästerby, and M. Lindgren, *Proceedings of SPIE* **5617** pp. 60-74 (2004).
7. T. Tjärnhage, M. Strömqvist, G. Olofsson, D. Squirrell, J. Burke, J. Ho, and M. Spence, *Field Analytical Chemistry & Technology* **5** (4), pp. 171-176 (2001).
8. P. H. Kaye, J. E. Barton, E. Hirst, and J. M. Clark, *Applied Optics* **39** (21), pp. 3738-3745 (2000).
9. J. Ho, *Analytica Chimica Acta* **457** (1), pp. 125-148 (2002).
10. V. Sivaprakasam, A. L. Houston, C. Scotto, and J. D. Eversole, *Optics Express* **12** (19), pp. 4457-4466 (2004).
11. R. G. Pinnick, S. C. Hill, Y.-L. Pan, R. K. Chang, *Atmospheric Environment* **38** (11), pp. 1657–1672 (2004).
12. M. Tiihonen, V. Pasiskevicius and F. Laurell, *Tailored UV-laser source for fluorescence spectroscopy of biomolecules*, accepted for publication in Special issue of Optics and Lasers in Engineering (2005).
13. V. Pasiskevicius, H. Karlsson, F. Laurell, R. Butkus, V. Smilgevicius, and A. Piskarskas, *Optics Letters* **26** (10), pp. 710-712 (2001).
14. D. J. Armstrong, A. V. Smith, *Proceedings of SPIE* **4893**, pp. 105-120 (2002).
15. J. R. Simard, G. Roy, P. Mathieu, V. Larochelle, J. McFee, and J. Ho. *IEEE Transactions on Geoscience and Remote Sensing* **42** (4), 865-874, (2004).
16. R. M. Measures, *Laser Remote Sensing: Fundamentals and Applications*, (New York, John Wiley & Sons, 1984).